PHYSICAL REVIEW B **92**, 140402(R) (2015)

Magnetothermoelectric power in Co/Pt layered structures: Interface versus bulk contributions

Axel Frauen, André Kobs, Tim Böhnert,* Ann-Kathrin Michel, Gerrit Winkler, Kornelius Nielsch, and Hans Peter Oepen
Institut für Nanostruktur- und Festkörperphysik, Universität Hamburg, Jungiusstraße 11, 20355 Hamburg, Germany
(Received 18 August 2014; published 2 October 2015)

The dependence of the longitudinal thermoelectric power on the orientation of magnetization in Pt/Co/Pt sandwiches is investigated. In the Co thickness range $\leqslant$6 nm, where interface scattering is relevant, the thermoelectric power depends on the orientation of magnetization in the plane perpendicular to the temperature gradient. This behavior reveals the thermoelectric analog to the anisotropic interface magnetoresistance. It is shown that this *interfacial* magnetothermoelectric power fulfills Mott's formula, however, significant deviations from the bulk anisotropic magnetothermoelectric behavior are reported. The dependence of the Seebeck effect on magnetization orientation therefore provides experimental evidence of differences in the electronic states of the bulk and interface. We demonstrate that for the very same system the Seebeck coefficient does not show a one-to-one correspondence to the conductivity.

DOI: 10.1103/PhysRevB.92.140402 PACS number(s): 75.47.−m, 72.15.Jf, 73.50.Jt, 75.70.−i

The topic of intense research known as *spin caloritronics* deals with the generation, detection, and quantification of spin currents in thin films arising from thermal gradients [1–4]. Spin currents are electrically detectable via the anomalous Hall (or Nernst) effect or inverse spin Hall effect due to spin-dependent scattering processes.

The investigation of galvanomagnetic effects (the interplay of charge and spin flow) and thermomagnetic phenomena (the interplay of heat and spin flow) in ferromagnetic metals has a long history, starting with studies in the 19th century [5]. The anisotropic magnetoresistance (AMR), for instance, was discovered in ferromagnetic 3*d* metals by Lord Kelvin in 1856 [6]. The resistivity varies as $\cos^2\varphi$, where φ is the angle between magnetization **M** and current direction. In general, it is largest for **M** oriented along the latter [7]. In the same year, Kelvin also discovered the magnetothermoelectric analog to the AMR, i.e., the anisotropic magnetothermoelectric power (anisotropic MTEP or AMTEP) [8].

The connection between the absolute thermoelectric power (Seebeck coefficient) S and electrical conductivity σ came to be known as the Mott formula [9–11],

$$S(\mathbf{M}) = \frac{\pi^2 k_B^2 T}{3e}\frac{1}{\sigma(\mathbf{M})}\left[\frac{\partial\sigma(E,\mathbf{M})}{\partial E}\right]_{E=E_F}, \qquad (1)$$

where T is the temperature, E_F is the Fermi energy, and k_B and e are the Boltzmann constant and elementary charge, respectively. The Mott formula is derived from the Boltzmann equation under the assumption of noninteracting electrons that scatter at randomly distributed defects of the crystal lattice [12,13]. Several representations of Mott's formula are found in the literature. The expression as given in Eq. (1) is motivated in the Supplemental Material, paragraph II [14]. Its validity has been numerously experimentally demonstrated [13,15–18]—even in the presence of magnetoresistance effects and magnetothermoelectric power—yielding a close relationship between galvanomagnetic and thermomagnetic phenomena. In particular, in the case of AMR [19–21], magnon MR [21–23], giant MR (GMR) [24–27], tunneling MR (TMR) [28], and their corresponding magnetothermoelectric equivalents, linear dependences of the Seebeck coefficient S on the inverse electrical conductivity $\sigma^{-1}(\mathbf{M})$ are found with the magnetization **M** as an implicit variable. Even for the transverse conductivity/thermoelectric power, which depends on **M** due to the anomalous Hall/Nernst effect, a similar relation was found [29–31].

In this Rapid Communication we report on the longitudinal magnetothermoelectric power and magnetoresistance of Co/Pt layered structures. In accordance with the literature, a linear dependence of S on $\sigma^{-1}(\varphi)$ is found when the orientation of magnetization is varied in the film plane (angle φ) with respect to the temperature gradient/direction of current flow (bulk AMTEP versus AMR). Besides the bulk AMR, the Co/Pt interfaces provide a further contribution to the magnetoresistance [32,33]. Due to the so-called anisotropic interface MR (AIMR), the resistivity varies with $\cos^2\theta$, where θ is the angle between the magnetization **M** and film normal, and is largest for **M** oriented out of plane [32,34]. The AIMR has been qualitatively modeled in a fully relativistic description of the magnetotransport [35] where the spin-orbit interaction is inherently included, and in a semiclassical Boltzmann approach taking the (interfacial) Bychkov-Rashba spin-orbit interaction into account [36]. In this study we have succeeded in identifying the thermoelectric equivalent of the AIMR. When changing **M** within the plane perpendicular to the temperature gradient (in zero applied electric field), the resulting $S(\theta)$ curve is again proportional to $\sigma^{-1}(\theta)$, in accordance with Mott's formula. The proportionality factor of S on σ^{-1}, however, is different for anisotropic interface and bulk scattering contributions.

The Co/Pt samples are grown by sputter techniques under ultrahigh vacuum conditions [37] on a glass substrate. Wires of a lateral size of 510 μm × 20 μm are fabricated by means of optical lithography. Additionally, a 60 nm thick Pt film is deposited and structured to create the electrical contacts, resistance thermometers, and heater [see the layout in Fig. 1(a)]. In order to unambiguously show the general validity of the results, we vary the volume to interface ratio, i.e., Pt(5 nm)/Co(t_{Co})/Pt(3 nm) stacks with different Co layer

*Present address: International Iberian Nanotechnology Laboratory (INL), Av. Mestre José Veiga, 4715-315 Braga, Portugal.

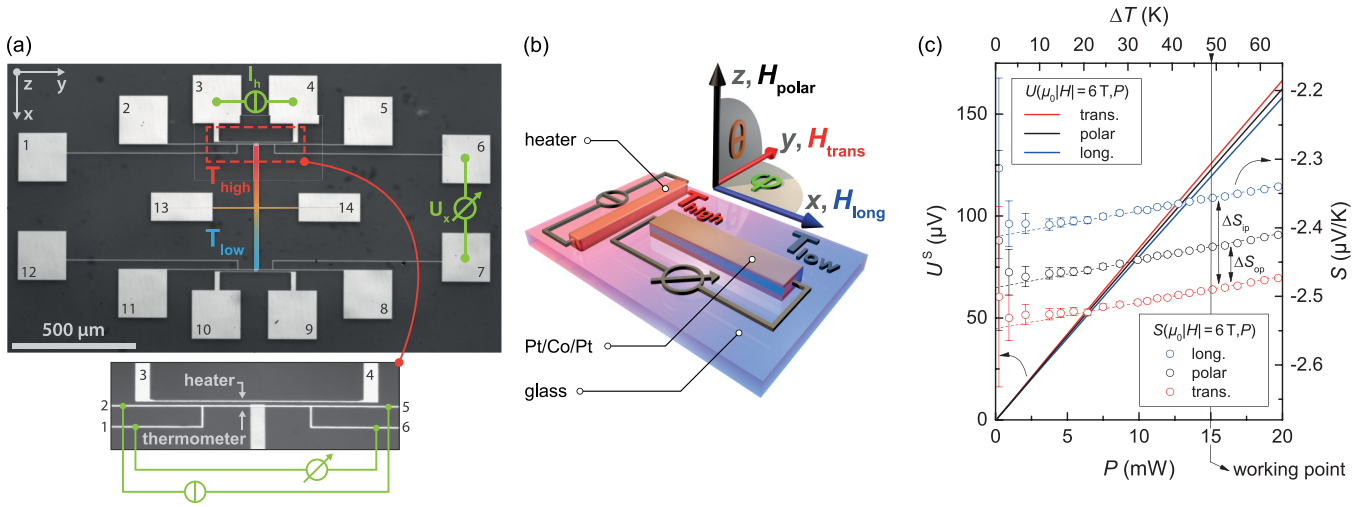

FIG. 1. (Color online) (a) Image of the microcircuit. For the MR measurements, the current along the vertically oriented Co/Pt wire is measured via contacts (6,7) for a constant voltage applied to the Pt pads (2,11). For the MTEP measurements, a temperature gradient along the Co/Pt wire is generated by driving a current through the Pt heater via contacts (3,4). The resulting thermovoltage U^S is measured via pads (6,7) [or (1,12)]. The upper heater and resistance thermometer including the circuit diagram for the temperature calibration are seen in the zoom in the lower panel. (b) Sketch of the microcircuit denoting the measuring geometries. $U^S(\mathbf{H})$ is determined for the field $\mathbf{H}$ oriented along the temperature difference ΔT (longitudinal), perpendicular to ΔT in the film plane (transverse), and out of plane (polar geometry), respectively. The $U^S(\mathbf{M})$ behavior is obtained by rotating the magnetization $\mathbf{M}$ in a saturation field of 6 T, varying $\mathbf{M}$ in the film plane (angle φ) and in the plane perpendicular to ΔT (angle θ), respectively. (c) U^S for the three generic orientations of the applied magnetic field ($\mu_0|H| = 6$ T) in dependence on ΔT/heating power P (solid lines), here shown for $t_{\mathrm{Co}} = 2$ nm. From the curves, the Seebeck coefficient $S = -U^S/\Delta T$ is extracted (circles). The dashed lines are linear fits to the curves for $P > 7$ mW. The differences $\Delta S_{\mathrm{ip}} = (U^S_{\mathrm{trans}} - U^S_{\mathrm{long}})/\Delta T$ and $\Delta S_{\mathrm{op}} = (U^S_{\mathrm{trans}} - U^S_{\mathrm{polar}})/\Delta T$ are indicated.

thicknesses are investigated. The sample with $t_{\mathrm{Co}} = 0.8$ nm ($t_{\mathrm{Co}} = 2$ and 6 nm) has an easy (hard) axis of magnetization along the film normal [37]. The structural properties of the samples are not influenced by the variation of Co thickness in this range [37]. Hence, the different easy axis only changes the magnetization reversal but plays no role for the discussion of the size of the MR and MTEP effects.

The investigations of MR and MTEP are performed at room temperature using magnetic fields of up to ±6 T. The longitudinal conductivity σ is determined via a four point measurement geometry applying a fixed voltage in the range of 1–2 V [Fig. 1(a); for details, see Supplemental Material, paragraph I [14]]. The thermovoltage U^S is measured using a heating power of maximum $P = 20$ mW that is applied to the Pt heater, creating a temperature difference of maximum $\Delta T = (63.7 \pm 0.5)$ K with $T_{\mathrm{low}} \approx 295.5$ K. To calibrate the temperature difference ΔT versus power P, the resistance of the two Pt thermometers is measured in four point geometry when varying the temperature of the whole device between 290 and 360 K (at $P = 0$ mW) [38]. It turns out that the temperature difference is proportional to the heating power [see both abscissas in Fig. 1(c)] with an error margin of <3%. The longitudinal thermovoltage U^S as a function of ΔT is measured for the three generic orientations of the external magnetic field [see the sketch in Fig. 1(b)]. As can be seen in Fig. 1(c), U^S apparently depends linearly on ΔT. When plotting $S = -U^S/\Delta T$ versus ΔT, however, it becomes obvious that there is a constant contribution as well as a contribution that causes a linear increase of S with ΔT. For all three orientations of the magnetic field, however, the slope is identical within the error margins of the experiment. This implies that the MTEP results presented in the following for $\Delta T \approx 49$ K are valid for a wide range of temperature differences, especially for the limiting case $\Delta T \to 0$ that formally defines the thermoelectric power $S(T = 294\ \mathrm{K}, \mathbf{M}, \mathbf{H}) = \lim_{\Delta T \to 0} \frac{-U^S(\mathbf{M},\mathbf{H})}{\Delta T}$ [13,39]. It is worth mentioning that S is the difference in thermopowers of the Pt/Co/Pt wire and Pt contacts [40]. In the Supplemental Material [14] (paragraph III) it is shown, however, that $S(\mathbf{M},\mathbf{H}) \propto S_{\mathrm{Co}}(\mathbf{M},\mathbf{H})$ is a good approximation when dealing with MTEP contributions. Contributions from the Nernst effect [41] (transverse MTEP contributions) are superimposed on the signal, which makes a detailed analysis necessary (see paragraph IV of the Supplemental Material [14]).

In Fig. 2(a) the longitudinal inverse conductivity, i.e., the longitudinal resistivity (see Supplemental Material, paragraph I [14]), versus magnetic field is given for the three generic field orientations for the Pt/Co/Pt wire with Co thickness $t_{\mathrm{Co}} = 2$ nm [see the sketch in Fig. 1(b)]. For this sample the magnetic hard axis is the film normal, which causes a parabolalike behavior of the polar sweep $1/\sigma(H_{\mathrm{polar}})$ [42]. The latter is due to the angle dependence of the AMR and AIMR and a coherent rotation of magnetization which is completed at ≈1 T. The steep resistivity changes at small fields (<100 mT) observed for the longitudinal and transverse field sweeps are due to the magnetization reversal via domain wall movement. At technical saturation all curves merge into the same linear behavior, i.e., a decrease of inverse conductivity on an increase of field strength caused by magnon MR [43,44]. As a consequence of the isotropic high field

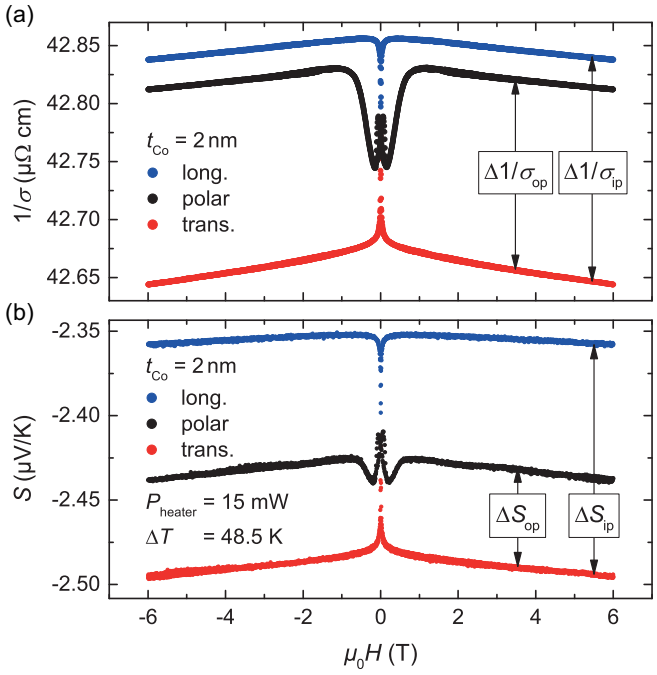

FIG. 2. (Color online) Field sweep measurements for the Pt/Co(2 nm)/Pt sandwich. (a) Inverse conductivity $1/\sigma$ and (b) Seebeck coefficient S as a function of applied field $\mu_0 H$ for the three principle directions of the field with respect to the electric field direction/temperature gradient and film normal [see Fig. 1(b)]. The difference in inverse conductivity and Seebeck coefficient above technical saturation are labeled as $\Delta\sigma_{ip}^{-1} = \sigma_{long}^{-1} - \sigma_{trans}^{-1}$ (AMR) and $\Delta\sigma_{op}^{-1} = \sigma_{polar}^{-1} - \sigma_{trans}^{-1}$ (AIMR), and $\Delta S_{ip} = |S_{trans}| - |S_{long}|$ (AMTEP), $\Delta S_{op} = |S_{trans}| - |S_{polar}|$ (interfacial AMTEP), respectively.

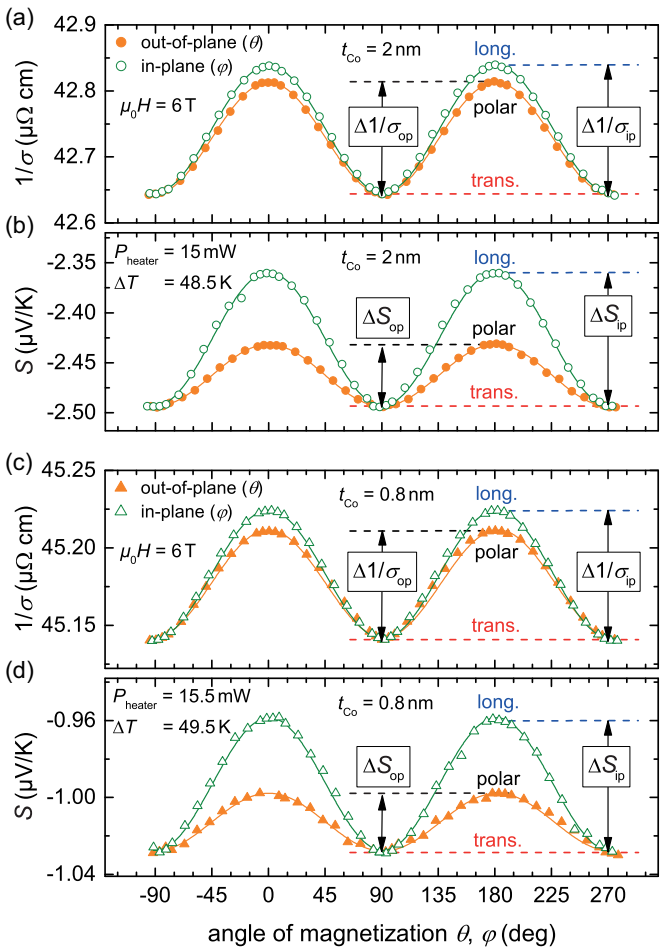

FIG. 3. (Color online) Inverse conductivity $1/\sigma$ and Seebeck coefficient S versus magnetization orientation. (a) and (b) show the results for Pt/Co(2 nm)/Pt and (c) and (d) for Pt/Co(0.8 nm)/Pt. φ and θ are the in-plane and out-of-plane angles of **M** with respect to the electric field and film normal, respectively [see Fig. 1(b)]. The field strength is 6 T, causing **M** to be field aligned. The solid lines represent $\cos^2$ fits. The amplitudes are labeled according to Fig. 2.

behavior, the differences $\Delta\sigma_{ip}^{-1} = \sigma_{long}^{-1} - \sigma_{trans}^{-1}$ (AMR) and $\Delta\sigma_{op}^{-1} = \sigma_{polar}^{-1} - \sigma_{trans}^{-1}$ (AIMR) [32,34] are constant above saturation and are equal to the differences in $1/\sigma$ extrapolated from high field behavior to zero field.

The corresponding magnetothermoelectric measurements of the very same sample ($t_{Co} = 2$ nm) are given in Fig. 2(b). Qualitatively, each individual plot of the Seebeck coefficient $S = -U^S/\Delta T$ versus field resembles the corresponding $1/\sigma(\mathbf{H})$ curve, which indicates that $S(\mathbf{M})$ is proportional to $1/\sigma(\mathbf{M})$. Above technical saturation, the absolute values of the three MTEP curves exhibit the following relation of Seebeck coefficients: $|S_{trans}| > |S_{polar}| > |S_{long}|$. Due to the isotropic high field behavior, the differences between the curves are again constant above saturation. The magnetothermoelectric power due to the AMR of Co is given by $\Delta S_{ip} = |S_{trans}| - |S_{long}|$ (AMTEP) while the difference $\Delta S_{op} = |S_{trans}| - |S_{polar}|$ is also distinctly larger than zero, revealing the existence of the magnetothermoelectric equivalent of the AIMR.

The isotropic high field behavior of the inverse conductivity and Seebeck coefficient (Fig. 2) allows for the determination of $1/\sigma(\mathbf{M})$ and $S(\mathbf{M})$ by rotating the samples in a saturation field of $\mu_0|H| = 6$ T. The latter field is high enough to keep **M** aligned with any direction of field. The inverse conductivity as a function of the orientation of **M** is given in Fig. 3(a) for $t_{Co} = 2$ nm. The characteristic $\cos^2\varphi$ dependence of the AMR effect is revealed for in-plane rotation, $1/\sigma(\varphi)_{\theta=90^\circ}$ (open green symbols). The same functional behavior of inverse conductivity is found for a rotation of magnetization in the plane perpendicular to the direction of electric field, $1/\sigma(\theta)_{\varphi=90^\circ}$ (AIMR), where θ denotes the orientation of magnetization to the film normal (solid orange symbols). The corresponding MTEP measurements are plotted in Fig. 3(b). The curves qualitatively resemble the angle dependence of the MR curves, namely, a $\cos^2$ behavior for both kinds of magnetization rotations $S(\varphi,\theta)$, which is consistent with the Mott formula for both rotational geometries. Consequently, $S(\varphi)_{\theta=90^\circ}$ shows the conventional bulk anisotropic MTEP described in the literature [20] with an amplitude of $\Delta S_{ip} = |S_{trans}| - |S_{long}|$ (green curve), while the anisotropy in the plane perpendicular to the temperature gradient $S(\theta)_{\varphi=90^\circ}$ with $\Delta S_{op} = |S_{trans}| - |S_{polar}| > 0$ stands for the magnetothermoelectric counterpart of the AIMR (orange curve),

$$S(\varphi,\theta) = S_{trans} + \Delta S_{ip}\cos^2\varphi\sin^2\theta + \Delta S_{op}\cos^2\theta. \quad (2)$$

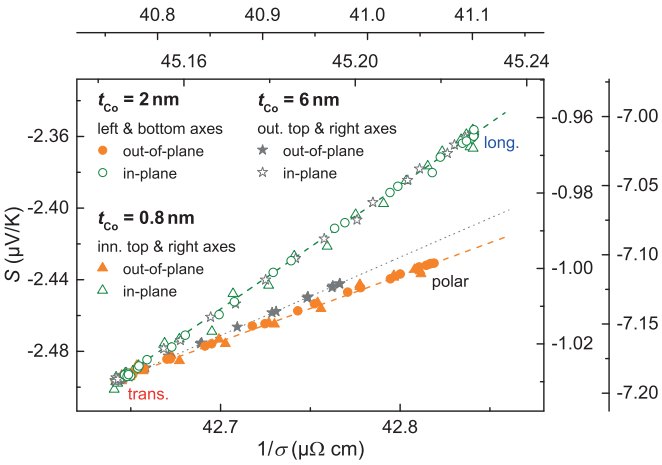

FIG. 4. (Color online) Seebeck coefficient S versus inverse electrical conductivity $1/\sigma$. The magnetization is rotated in plane (open symbols) and out of plane (solid symbols). The triangles, circles, and stars represent the Co thicknesses of 0.8, 2, and 6 nm, respectively. The dashed/dotted lines are linear fits to the data (0.8 nm, 2 nm/6 nm).

To stress the point, the latter magnetothermoelectric effect locally probes the Co/Pt interface region and exhibits the same functional dependence on inverse conductivity as in the case of bulk properties.

Obviously, the interfacial effect (out-of-plane rotation) with respect to the bulk effect (in-plane rotation) is larger in the MR than in the MTEP: $\Delta\sigma_{op}^{-1}/\Delta\sigma_{ip}^{-1} > \Delta S_{op}/\Delta S_{ip}$. For the sake of better comparison, the Seebeck coefficient $S(\varphi,\theta)$ is mapped onto the inverse conductivity $\sigma^{-1}(\varphi,\theta)$ (Fig. 4). Both $S(\varphi)$ and $S(\theta)$ curves are directly proportional to $\sigma^{-1}(\varphi)$ and $\sigma^{-1}(\theta)$ (open/solid circles), respectively, while the linear plots have different slopes. The interfacial contribution $S(\sigma^{-1}(\theta))$ has a smaller slope. Quantitatively, $(\Delta S_{op}/\Delta\sigma_{op}^{-1})/(\Delta S_{ip}/\Delta\sigma_{ip}^{-1}) = (0.53 \pm 0.02)$.

As a cross check, a sandwich with a very thin Co layer ($t_{Co} = 0.8$ nm) has been investigated. The angular dependences of $\sigma^{-1}(\varphi)$ and $\sigma^{-1}(\theta)$, and $S(\varphi)$ and $S(\theta)$ on magnetization orientation are shown in Figs. 3(c) and 3(d), respectively. The plots are very similar to the one for $t_{Co} = 2$ nm. Quantitatively, $(\Delta S_{op}/\Delta\sigma_{op}^{-1})/(\Delta S_{ip}/\Delta\sigma_{ip}^{-1}) = (0.52 \pm 0.02)$ is found, which is the same value within the error margins as found for $t_{Co} = 2$ nm (see Fig. 4). Hence, the scaling of the **M** dependent contributions to the thermopower on inverse conductivity is different for the bulk and interface but independent of Co thickness, revealing the generality of our finding. Note that this finding is also a consequence of the fact that the system can be treated as an isolated Co single layer with the bulk and interfacial MR and MTEP effects when dealing with the ratios $(\Delta\sigma_{op}^{-1}/\Delta\sigma_{ip}^{-1})$ [32] and $(\Delta S_{op}/\Delta S_{ip})$. In the case of the latter, the impact of the layered structure cancels out in a first approximation for small t_{Co}, as shown in a detailed analysis for layered structures (parallel wires) presented in the Supplemental Material, paragraph III [14]. For higher Co thicknesses ($t_{Co} \gtrsim 5$ nm), however, a correction is essential. For a sample with $t_{Co} = 6$ nm, a value of (0.63 ± 0.02) is found for the ratio $(\Delta S_{op}/\Delta\sigma_{op}^{-1})/(\Delta S_{ip}/\Delta\sigma_{ip}^{-1})$ (see the star symbols in Fig. 4). Utilizing the **M** dependent correction factor (see the Supplemental Material, paragraph III [14]), the value reduces to about 0.5, which is a further indication for the generality. For even larger Co thicknesses the situation is more complex as bulk effects in $\Delta\sigma_{op}^{-1}$ (and ΔS_{op}) such as the so-called geometrical size effect (GSE) [45] show up and become dominant for $t_{Co} \gtrsim 20$ nm [32]. Hence, the ratio $(\Delta S_{op}/\Delta\sigma_{op}^{-1})/(\Delta S_{ip}/\Delta\sigma_{ip}^{-1})$ will vary with Co thickness. In addition, for small $|\Delta S_{op}|$ a proper correction for Nernst effects becomes challenging.

In conclusion, it is proven that the scattering anisotropy of polarized electrons at the interfaces has an impact on the longitudinal magnetothermoelectric power [Eq. (2)]. The Seebeck coefficient S depends linearly on the inverse electrical conductivity σ^{-1} (AIMR effect) in accordance with Mott's formula [Eq. (1)]. The slope of S versus σ^{-1} for the interface contribution is about half the value that is found for the bulk behavior, whereas the latter is probed by the AMR and anisotropic magnetothermoelectric power. As the slope of $S(\sigma^{-1}(\mathbf{M}))$ is proportional to the derivative $[\partial\sigma(E,\mathbf{M})/\partial E]_{E=E_F}$ [Eq. (1)], the different behavior of bulk and interface MTEP contributions reveals significant differences in the band structure of the Co layer at the interfaces compared to the bulk. In order to support this interpretation, layer resolved first principles calculations of electronic states in the Co/Pt system in dependence of magnetization orientation are needed [46,47]. A further contribution to the different slopes may arise from different strengths and types of spin-orbit coupling effects, giving rise to the AMR and AIMR effect [48]. The existence of differences in the bulk and interface effects prevents a one-to-one correlation between the Seebeck coefficient and conductivity for the very same system, so that for a given electrical conductivity that can be set either by the AMR or AIMR (Fig. 4), the resulting Seebeck coefficient can be tuned on purpose. The presented approach to independently probe the properties of the bulk and interfaces by means of MR and MTEP is not limited to Co/Pt layered structures, as the AIMR seems to be a general phenomenon that is present in a variety of layered structures [32,33,49,50].

Financial support by Deutsche Forschungsgemeinschaft via Project No. OE 251/7-1 "Investigation of the influence of interfaces on the magnetotransport in ultrathin films" and SFB 668 is gratefully acknowledged. We would like to thank J. Gooth for fruitful discussions.

[1] K. Uchida, S. Takahashi, K. Harii, J. Ieda, W. Koshibae, K. Ando, S. Maekawa, and E. Saitoh, Nature (London) **455**, 778 (2008).

[2] A. Slachter, F. L. Bakker, J.-P. Adam, and B. J. van Wees, Nat. Phys. **6**, 879 (2010).

[3] G. E. W. Bauer, E. Saitoh, and B. J. van Wees, Nat. Mater. **11**, 391 (2012).

[4] H. Adachi, K.-i. Uchida, E. Saitoh, and S. Maekawa, Rep. Prog. Phys. **76**, 036501 (2013).

[5] L. L. Campbell, *Galvanomagnetic and Thermomagnetic Effects—The Hall and Allied Phenomena* (Longmans, Green and Company, London, 1923).
[6] W. Thomson, Proc. R. Soc. London **8**, 546 (1856).
[7] T. R. McGuire and R. I. Potter, IEEE Trans. Magn. **11**, 1018 (1975).
[8] W. Thomson, Philos. Trans. R. Soc. London **146**, 649 (1856).
[9] N. F. Mott, Proc. R. Soc. London, Ser. A **156**, 368 (1936).
[10] M. Cutler and N. F. Mott, Phys. Rev. **181**, 1336 (1969).
[11] M. Stearns, in *Magnetic Properties of Metals*, edited by H. P. J. Wijn, Landolt-Börnstein, New Series, Group III, Vol. 19, Pt. A (Springer, Berlin, 1986).
[12] M. Jonson and G. D. Mahan, Phys. Rev. B **21**, 4223 (1980).
[13] F. J. Blatt, P. A. Schroeder, C. L. Foiles, and D. Graig, *Thermoelectric Power of Metals* (Plenum, New York, 1976).
[14] See Supplemental Material at http://link.aps.org/supplemental/10.1103/PhysRevB.92.140402 for details of conductivity measurements (I), the Mott formula (II), influence of the layered structure on MTEP (III), and parasitic contributions in longitudinal MTEP measurements (IV).
[15] A. V. Gold, D. K. C. Macdonald, W. B. Pearson, and I. M. Templeton, Philos. Mag. **5**, 765 (1960).
[16] J. P. Small, K. M. Perez, and P. Kim, Phys. Rev. Lett. **91**, 256801 (2003).
[17] Y. M. Zuev, W. Chang, and P. Kim, Phys. Rev. Lett. **102**, 096807 (2009).
[18] A. D. Avery, R. Sultan, D. Bassett, D. Wei, and B. L. Zink, Phys. Rev. B **83**, 100401 (2011).
[19] J.-E. Wegrowe, Q. A. Nguyen, M. Al-Barki, J.-F. Dayen, T. L. Wade, and H.-J. Drouhin, Phys. Rev. B **73**, 134422 (2006).
[20] A. D. Avery, M. R. Pufall, and B. L. Zink, Phys. Rev. B **86**, 184408 (2012).
[21] T. Böhnert, V. Vega, A.-K. Michel, V. M. Prida, and K. Nielsch, Appl. Phys. Lett. **103**, 092407 (2013).
[22] G. N. Grannemann and L. Berger, Phys. Rev. B **13**, 2072 (1976).
[23] M. V. Costache, G. Bridoux, I. Neumann, and S. O. Valenzuela, Nat. Mater. **11**, 199 (2012).
[24] F. Tsui, B. Chen, D. Barlett, R. Clarke, and C. Uher, Phys. Rev. Lett. **72**, 740 (1994).
[25] H. Sato, H. Henmi, Y. Kobayashi, Y. Aoki, H. Yamamoto, T. Shinjo, and V. Sechovsky, J. Appl. Phys. **76**, 6919 (1994).
[26] J. Shi, K. Pettit, E. Kita, S. S. P. Parkin, R. Nakatani, and M. B. Salamon, Phys. Rev. B **54**, 15273 (1996).
[27] S. Serrano-Guisan, G. di Domenicantonio, M. Abid, J.-P. Abid, M. Hillenkamp, L. Gravier, J.-P. Ansermet, and C. Félix, Nat. Mater. **5**, 730 (2006).
[28] N. Liebing, S. Serrano-Guisan, K. Rott, G. Reiss, J. Langer, B. Ocker, and H. W. Schumacher, Phys. Rev. Lett. **107**, 177201 (2011).
[29] T. Miyasato, N. Abe, T. Fujii, A. Asamitsu, S. Onoda, Y. Onose, N. Nagaosa, and Y. Tokura, Phys. Rev. Lett. **99**, 086602 (2007).
[30] Y. Pu, D. Chiba, F. Matsukura, H. Ohno, and J. Shi, Phys. Rev. Lett. **101**, 117208 (2008).
[31] R. Ramos, M. H. Aguirre, A. Anadón, J. Blasco, I. Lucas, K. Uchida, P. A. Algarabel, L. Morellón, E. Saitoh, and M. R. Ibarra, Phys. Rev. B **90**, 054422 (2014).
[32] A. Kobs, S. Heße, W. Kreuzpaintner, G. Winkler, D. Lott, P. Weinberger, A. Schreyer, and H. P. Oepen, Phys. Rev. Lett. **106**, 217207 (2011).
[33] J.-C. Lee, C.-H. Hsieh, C.-C. Chang, L.-W. Huang, L.-K. Lin, and S.-F. Lee, J. Appl. Phys. **113**, 17C714 (2013).
[34] A. Kobs, A. Frauen, and H. P. Oepen, Phys. Rev. B **90**, 016401 (2014).
[35] A. Kobs, S. Heße, H. Oepen, and P. Weinberger, Philos. Mag. **92**, 2835 (2012).
[36] S. S.-L. Zhang and S. Zhang, J. Appl. Phys. **115**, 17C703 (2014).
[37] G. Winkler, A. Kobs, A. Chuvilin, D. Lott, A. Schreyer, and H. P. Oepen, J. Appl. Phys. **117**, 105306 (2015).
[38] For the upper Pt wire (see the zoom in Fig. 1(a)) a noninvasive current of $I = 0.2$ mA is impressed via the leads (2,5), while (1,6) are the leads for the voltage measurement according to the circuit diagram in the zoom; lower wire accordingly: current (8,11), voltage (7,12).
[39] C. L. Foiles, in *Metals: Electronic Transport Phenomena*, edited by K.-H. Hellwege and J. L. Olsen, Landolt-Börnstein, New Series, Group III, Vol. 15, Pt. B (Springer, Berlin, 1985).
[40] R. D. Barnard, *Thermoelectricity in Metals and Alloys* (Taylor & Francis, London, 1972).
[41] W. Nernst, Ann. Phys. **267**, 760 (1887).
[42] The deviations from the parabolic shape of the polar curves are consequences of small misalignments of the magnetic field direction with respect to the film normal [32].
[43] B. Raquet, M. Viret, E. Sondergard, O. Cespedes, and R. Mamy, Phys. Rev. B **66**, 024433 (2002).
[44] V. D. Nguyen, L. Vila, P. Laczkowski, A. Marty, T. Faivre, and J. P. Attané, Phys. Rev. Lett. **107**, 136605 (2011).
[45] W. Gil, D. Görlitz, M. Horisberger, and J. Kötzler, Phys. Rev. B **72**, 134401 (2005).
[46] B. G. Park, J. Wunderlich, D. A. Williams, S. J. Joo, K. Y. Jung, K. H. Shin, K. Olejnik, A. B. Shick, and T. Jungwirth, Phys. Rev. Lett. **100**, 087204 (2008).
[47] V. Popescu and P. Kratzer, Phys. Rev. B **88**, 104425 (2013).
[48] J. Borge, C. Gorini, and R. Raimondi, Phys. Rev. B **87**, 085309 (2013).
[49] Y. M. Lu, J. W. Cai, S. Y. Huang, D. Qu, B. F. Miao, and C. L. Chien, Phys. Rev. B **87**, 220409 (2013).
[50] Y. Kachlon, N. Kurzweil, and A. Sharoni, J. Appl. Phys. **115**, 173911 (2014).